arXiv:cond-mat/0205547v1 [cond-mat.dis-nn] 27 May 2002

Characterization of the complex ion dynamics in lithium silicate glasses via computer simulations

Andreas Heuer, Magnus Kunow, Michael Vogel, and Radha D. Banhatti,

Institute of Physical Chemistry, Schlossplatz 4/7, D-48149 Münster

and Sonderforschungsbereich 458

andheuer@uni-muenster.de
kunow@uni-muenster.de
mivogel@uni-muenster.de
banhatt@uni-muenster.de

March 22, 2022

We present results of molecular dynamics simulations on lithium metasilicate over a broad range of temperatures for which the silicate network is frozen in but the lithium ions can still be equilibrated. The lithium dynamics is studied via the analysis of different correlation functions. The activation energy for the lithium mobility agrees very well with experimental data. The correlation of the dynamics of adjacent ions is weak. At low temperatures the dynamics can be separated into local vibrational dynamics and hopping events between adjacent lithium sites. The derivative of the mean square displacement displays several characteristic time regimes. They can be directly mapped onto respective frequency regimes for the conductivity. In particular it is possible to identify time regimes dominated by localized dynamics and long-range dynamics, respectively. The question of time-temperature superposition is discussed for the mean square displacement and the incoherent scattering function.

1 Introduction

The dynamics of ions in amorphous materials is very complex, as indicated, e.g., by the strong frequency dependence of the conductivity [1, 2, 3, 4]. This frequency dependence directly reflects the presence of back- and forthdynamics of the individual ions. The complexity of the

ion dynamics is due to the simultaneous action of the time-dependent Coulomb interaction with the other mobile ions and the time-independent interaction with the spatially disordered and basically immobile network. Interestingly, the frequency dependence of the conductivity is very similar when comparing different materials [1]. Even simulations of disordered hopping models display a similar frequency dependence; see, e.g., [2, 5, 6].

Typically the frequency-dependence of the conductivity $\sigma(\nu)$ displays several characteristic time regimes. For a sodium silicate system [7] one observes, e.g., a microsopic regime for $\nu > 10^{13}$ Hz, a scaling regime $\sigma(\nu) \propto \nu^2$ for 10^{13} Hz $> \nu > 10^{11}$ Hz, and finally for $\nu < 10^{11}$ Hz a continuous decrease of $\sigma(\nu)$ with decreasing ν. In a double-logarithmic representation at low temperatures the apparent exponent decreases from one to zero until the d.c. plateau is reached, i.e. $\sigma(\nu) = \sigma_{d.c.}$. A possible interpretation of this behavior relates these frequency regimes to local vibrations, stochastic localized dynamics, and jump dynamics, respectively [8]. An important observation for the frequency-dependent conductivity $\sigma(\nu)$ is the validity of the time-temperature superposition principle. For most materials it can be expressed by the Summerfield scaling for which $\sigma(\nu)/\sigma_{dc}$ is only a function of $\nu/(T\sigma_{dc})$ [9].

It is important to relate the frequency dependence of $\sigma(\nu)$ to the real space dynamics of the ions. In this way one may get interesting information about the nature of the ion dynamics. This can be done by expressing $\sigma(\nu)$ in terms of the mean square displacement $\langle r^2(t)\rangle$. Conceptually, both observables differ in one important aspect. While the conductivity contains effects of multi-particle correlations, the mean square displacement is a single-particle quantity. Experimentally, the correlation is expressed by the Haven ratio [10, 11] which in general can be frequency dependent (denoted $H_R(\nu)$). The experiments indicate that the correlation among different ions is small and furthermore can be approximated by a value H_R. $1/H_R$ is a measure for the number of ions which are significantly correlated. Then one can relate $\sigma(\nu)$ to $\langle r^2(t)\rangle$ via linear response theory [1, 12]

$$\sigma(\nu) = \frac{q^2}{6H_R\rho k_B T}\int_0^\infty dt\,(d/dt)w(t)\cos(2\pi\nu t) \tag{1}$$

where q denotes the charge, ρ the density of the mobile ions, and H_R the Haven ratio. The function $w(t)$ is defined as

$$w(t) = (d/dt)\langle r^2(t)\rangle. \tag{2}$$

Analysis of spatial aspects of dynamical processes is one of the strongholds of computer simulations. Here it is of particular help that detailed information is available on a microscopic level. Conceptually, one can proceed in two steps. In a first step one can study $w(t)$. On the basis of Eq.1 it has been readily shown that for a significant dispersion of the conductivity the frequency-dependence of $\sigma(\nu)$ and the time-dependence of $w(t)$ are basically mirror images of each other when identifying t with $1/\pi^2\nu$ [1]. Therefore it is the quantity $w(t)$ which is of uttermost importance for the direct relation to conductivity experiments since one may hope

to recover the three regimes of $\sigma(\nu)$ also in $w(t)$. As a consequence of Eq.1 a dispersion in $\sigma(\nu)$ is equivalent to a time dependence of $w(t)$ and a scaling relation $w(t) \propto t^{-\alpha}$ transfers to $\sigma(\nu) \propto \nu^{\alpha}$. In a second step one can analyse the dynamics in more detail to elucidate the underlying physical processes in the different time regimes. Although interesting details may be seen from the analysis of individual trajectories a sound understanding of the dynamics should be based on the study of appropriate correlation functions, yielding the *average* dynamical behavior.

In this paper we present computer simulations for lithium silicate following this general approach. As an example we take the lithium dynamics in $(Li_2O)(SiO_2)$ [13, 14, 15]. In contrast to most earlier work on this system the present computer generation allows one to study the lithium dynamics in the low-temperature dispersive regime in equilibrium conditions. Similar systems like sodium silicate systems are also of current interest for numerical studies [16, 17, 18, 19, 20, 21, 22, 23, 24, 25]. The outline of this paper is as follows. In Section 2 we describe the technical aspects of the simulation and discuss the numerical tools. The results of our simulations as well as their interpretation are presented in Section 3. We close with a discussion and a summary in Section 4.

2 Simulation

The potential energy of the lithium silicate system can be written as the sum of a Buckingham and Coulomb pair potential

$$U_{ij}(r) = \frac{q_i q_j e^2}{r} - \frac{C_{ij}}{r^6} + A_{ij} \exp(-B_{ij} r). \tag{3}$$

The pair indices i,j characterize the various ion pairs (Li-Li, Li-Si, etc.). The individual potential parameters are listed in our previous work [26]. They are based on the work of Habasaki et al. [13, 14, 27, 28, 29] and have been obtained from ab-initio calculations. Effective charges $q_{Si} = 2.4, q_{Li} = 0.87$, and $q_O = 1.38$ have been chosen. This choice fulfills charge neutrality of the total system. Periodic boundary conditions have been used. Simulations during the production runs were performed in the NVE ensemble. The elementary timestep of our molecular dynamics simulations was 2 fs, the density $\rho = 2.34$ g cm^{-3}, taken from experimental room temperature data [30]. This corresponds to pressures of the order of 1 GPa at the lowest temperatures of our simulation. The total number of atoms in our system is 1152. For generating the trajectories we have used the programm MOLDY, supplied by K. Refson [31]. In our longest simulation run the system has been propagated for 20 ns. For our simulations we have started from configurations at T = 1500 K where ions as well as network could be equilibrated. Equilibration of the total system at this temperature requires a simulation run of ca. 4 ns. We note that the computer glass transition as observed on the time scale of 10 ns is approximately 1100 K (see network

diffusion data in [26]). In the present simulation we have chosen one temperature slightly above T_g (T = 1240 K) and four temperatures below T_g (T = 980 K, 750 K, 700 K, and 640 K). For these four temperatures we have paid attention to equilibrate the lithium subsystem before recording our observables. The network only performs local fluctuations with an average radius much smaller than one Angstrom. Interestingly, despite this fact we observed a slight temperature drift as a result of the continuous relaxation of the network for temperatures below the glass transition.

3 Results

3.1 Trajectories

In Fig.1 some representative trajectories of individual lithium ions at $T = 750$ K are shown. For these ions the dynamics can be described as a series of local vibrations and jumps between adjacent ionic sites. Similar features have been observed in several previous simulations on alkali silicates, see e.g. Refs. [22, 23, 24]. The three ions, displayed in Fig.1, behave somewhat differently. Whereas ion (1) does not leave its intitial site at all, ion (2) performs several back- and forthjumps between two adjacent sites, and ion (3) follows a random-walk like path between adjacent sites. The variety of different motional patterns directly shows that it is important to use appropriate statistical observables to identify the average type of behavior of the lithium dynamics. This is the subject of the remainder of the paper.

3.2 Structure

In Fig.2 we display the partial Li-Li structure factor $g(r)$ for several temperatures. One can clearly see that $g(r)$ shows a sharp nearest neighbor peak at $r_{nn} \approx 2.6$ Å. Interestingly, the width of the nearest-neighbor peak of $g(r)$ only slightly changes in the temperature range between $T = 750$ K and $T = 1240$ K. Here we have included also a very high temperature $T = 4000$ K from our previous simulations [26]. Only for the higher temperature the nearest neighbor peak broadens. This shows that the low-temperature width of the nearest-neighbor peak is mainly due to the disorder of the network and not due to thermal fluctuations in crystalline-like ionic sites.
To study the degree of clustering of the lithium ions we have calculated the function

$$h(r) = \frac{\int_0^r ds g(s) 4\pi s^2}{4\pi r^3/3}. \tag{4}$$

$h(r)$ counts the number of particles around a central particle in a sphere of radius r relative to the number one would have for a random distribution of particles. Thus the value of $h(r)$ is a

direct measure whether or not a particle is surrounded by more ($h(r) > 1$) or less ($h(r) < 1$) particles than expected for a random distribution. The first neighbor shell, as obtained from the first minimum of $g(r)$ ranges up to $r \approx 4.4$ Å. Therefore the value $h(r = 4.4$ Å$)$ yields information whether the number of particles in the nearest neighbor shell is smaller or larger than expected for a statistical distribution. The function $h(r)$ is displayed in Fig.3. It turns out that for low temperatures $h(r = 4.4$ Å$) \approx 0.9$. This indicates that the repulsion effect of the ions due to their mutual Coulomb interaction dominates the structure of the lithium subsystem. For $T = 4000$ K the distribution is essentially statistical, as expected for a dominance of entropic contributions. It is known experimentally from the study of alkali silicates [32, 33] that for smaller alkali concentration the alkali ions start to form clusters and indeed we observe in so far unpublished work that for $(Li_2O)9(SiO_2)$ $h(r = 4.4$ Å$) \approx 1.5$.

3.3 Dynamics

At first we would like to present results for the mean square displacement $\langle r^2(t)\rangle$ at different temperatures; see Fig.4. For all temperatures there exists a significant subdiffusive regime which is more pronounced for the lower temperatures. Note that at much higher temperatures the subdiffusive regime disappears and one observes a direct transition from a ballistic short-time regime $\langle r^2(t)\rangle \propto t^2$ to a diffusive long-time regime $\langle r^2(t)\rangle \propto t$ [26]. The diffusion constant D can be directly estimated from the long-time regime via $D = \langle r^2(t)\rangle/(6t)$.
Next we present the temperature dependence of the diffusion constant $D(T)$. The results are shown in Fig.5. We have included high-temperature data points as already presented in our previous work [26]. The dynamics is characterized by a single activation energy $E_a = 0.58$ eV in the temperature range between $T = 6000$ K and $T = 640$ K. The computer glass transition $T_g \approx 1100$ K does not show up in the temperature dependence of the diffusion constant because already above this temperature the ion and network dynamics are strongly decoupled.
For a comparison of the activation energy with experimental results one should consider constant pressure rather than constant density simulations. In order to check how much the above-mentioned value of E_a is modified we took the pressure of the T=1500 K run and checked how much the diffusion constant at T=6000 K is modified when using constant pressure rather than constant density. It turned out that the diffusion constant increased by a factor of 1.6. This corresponds to an increase of the activation energy by 0.08 eV, i.e. $\tilde{E}_a = 0.66$ eV. This value compares very well with the experimental value of 0.59 eV as obtained from conductivity experiments [34].
In Fig.6 we show that all curves can be superimposed on each other by substituting t by $t^* = (D(T)/D_0)t$ (The constant D_0 is chosen as $D(T = 640$ K$)$). Thus one may conclude that in the scaling regime, starting beyond the ballistic regime, $\langle r^2(t^*)\rangle$ fulfills the time-temperature superposition principle. The relation to the experimental findings will be discussed in the next Section.

From a theoretical perspective the incoherent scattering function $S(q,t)$ is an important observable to characterize the dynamics. It is defined as

$$S(q,t) = \langle \cos(\vec{q}(\vec{r}(t) - \vec{r}(0))) \rangle. \tag{5}$$

For isotropic systems it only depends on the absolute value q of the wave vector $\vec{q}$. In particular for $q = q_{max} = 2\pi/r_{nn}$ (in our case $q_{max} = 2.4$ Å^{-1}) one gets information about the dynamical processes on the lengthscale of nearest neighbor lithium distances. For glass forming liquids one can formulate a theory which characterizes the time and wave vector dependence of $S(q,t)$ for a broad range of temperatures [35]. In Fig.7 one can find $S(q_{max},t)$ at different temperatures. The decay time is an appropriate measure for the time scale on which an ion effectively moves to the next site.

For glass-forming liquids it is predicted from theory and confirmed by simulation that $S(q,t)$ follows the time-temperature superposition principle in the long-time regime [35, 36]. Interestingly, also for the present case of the lithium dynamics time-temperature superposition is observed. This can be seen from Fig.7 where at all temperatures $S(q_{max},t)$ is fitted to the Kohlrausch-Williams-Watts function $A\exp(-(t/\tau)^{\beta})$ with $\beta = 0.45$. Actually, the temperature dependence of τ is also activated (not shown). In the range of temperatures analysed in this work the variation of τ is four times larger than the variation of the diffusion constant. Thus translates into a higher activation energy of 0.70 eV rather than 0.58 eV as obtained for the diffusion constant. A possible origin of this descrepancy is discussed in the next Section.

The primary goal of this paper is to elucidate the nature of the frequency dependence of the conductivity. As already discussed the conductivity and the mean square displacement are directly related if the Haven ratio H_R is constant. This is particularly the case if H_R is close to one, i.e. dynamical inter-ion correlations are small. In recent work we have introduced a quantitity $N_{coop}(t)$ which is a measure of cooperativity on a time scale t [37]. It is defined as

$$N_{coop}(t) \equiv \frac{\sum_{ij} X_i(t) X_j(t)}{\sum_i X_i(t) X_i(t)} \tag{6}$$

where $X_i(t)$ is a dynamic property of ion i on the time scale t which on average is zero, i.e. $\sum_i X_i(t) = 0$. Here we choose

$$X_i(t) \equiv (\vec{r}_i(t) - \vec{r}_i(0))^2 - \langle r^2(t) \rangle. \tag{7}$$

For the practical implementation of this approach it is essential that N_{coop} is calculated for subsystems. The technical details of this analysis can be found in [37]. The results are shown in Fig.8. For a better comparison of the different temperatures we have plotted N_{coop} against the normalized time t^*. As expected $N_{coop}(t^*)$ approaches one on very short and very long time scales since the different ions behave independently. For all temperatures the maximum occurs at approximately the same scaled time $t^* \approx 500ps$. This time corresponds to the regime

where the transition from the strongly subdiffusive to the diffusive regime occurs. For the lower temperatures there are approximately 4 particles which are dynamically correlated. In contrast to glass-forming systems there is only a minor temperature dependence of N_{coop}. A further difference for glass-forming liquids is that the maximum value of N_{coop} can be larger than 20 close to the glass transition [37]. Therefore the present values of N_{coop} are indeed small.
Is N_{coop} related to the Haven ratio? On a qualitative level both quantities express the dynamic cooperativity. In the most simple case exactly $M \ll N$ particles behave identically but all these subsets of M particles behave in an uncorrelated manner. Then one simply has

$$N_{coop} = 1/H_R = M. \tag{8}$$

On a more quantitative level we start from the zero-frequeny limit of the Haven-ratio, thereby slightly extending the arguments given in [37]. This limit is given by

$$H_R = \frac{\sum_i \int_0^\infty dt \, \langle v_i(0) v_i(t) \rangle}{\sum_{i,j} \int_0^\infty dt \, \langle v_i(0) v_j(t) \rangle}. \tag{9}$$

These terms can be further rewritten in order to obtain the connection with N_{coop}. Due to time-reversal symmetry of the molecular dynamics one has $\langle v_i(0) v_j(t) \rangle = \langle v_i(0) v_j(-t) \rangle$. We define t_m as a time far in the diffusive long-time regime, i.e. much longer as the time t_d for which the velocity-correlations have basically decayed to zero. Then one can write

$$\int_0^\infty dt \, \langle v_i(0) v_j(t) \rangle = (1/2) \int_{-t_m}^{t_m} dt \, \langle v_i(0) v_j(t) \rangle. \tag{10}$$

For $-t_m + t_d < \tau < t_m - t_d$ one can substitute $v_i(0)$ by $v_i(\tau)$. Thus, for $t_m \to \infty$ one can write

$$\int_{-t_m}^{t_m} dt \, \langle v_i(0) v_j(t) \rangle = (1/2t_m) \int_{-t_m}^{t_m} d\tau \int_{-t_m}^{t_m} dt \, \langle v_i(\tau) v_j(t) \rangle. \tag{11}$$

For stationary processes one can substitute the integration limits by 0 and $2t_m$, respectively. Rewriting Eq.9 in terms of the above relations and replacing $\int_0^{2t_m} dt \, v_i(t)$ by $r_i(2t_m) - r_i(0)$ one ends up by $H_R = 1/N_{coop}(t \to \infty)$ when choosing $X_i(t) = \vec{r}_i(t) - \vec{r}_i(0)$. Thus Eq.8 also holds more generally. Unfortunately, for the present data the statistical error was very large with this choice of $X_i(t)$ and much smaller with the choice in Eq.7. However, for the hard sphere system analysed in [37] it turned out that to a very good approximation the maximum of $N_{coop}(t)$ with time for a quantity involving the absolute value of the shift vectors (like the one used above) is very close to the long-time limit of N_{coop} for the choice $X_i(t) = \vec{r}_i(t) - \vec{r}_i(0)$. Thus the maximum value of N_{coop} in Fig.8 is indeed a good measure for the inverse zero-frequency Haven ratio. Of course, a more detailed analysis of this aspect would be desirable. The resulting low-temperature estimate $H_R \approx 1/4$ is in agreement with typical experimental values [11]. Finally

we would like to mention that even this modest cooperativity has been stressed as a key feature to understand the long-time diffusion [38].
For a closer discussion of $w(t)$ (and thus of $\sigma(\nu)$) it will turn out to be helpful to use additional information about the real-space dynamics. For this purpose we have determined the van-Hove self-correlation function $G_s(r,t)$ for the lithium ions [39]

$$G_s(r,t) \equiv \langle \delta(r - |(\vec{r}(t) - \vec{r}(0))|) \rangle. \tag{12}$$

It denotes the probability that a lithium ion moves a distance r during the time t. The results are shown in Fig.9. One can clearly see that at short times the dynamics of all ions is confined to a small r-range. Of course, for longer times the ions may explore larger regions of the system. The presence of the first well-resolved peak around $d_0 \approx 2.6$ Å shows that hopping processes with jump length d_0 are a relevant feature of the dynamics. To a good approximation d_0 is identical to the r-value r_{nn} of the first nearest-neighbor peak of the partial structure factor $g(r)$. Also the other peaks of the partial structure factor show up in $G_s(r,t)$. Thus one may conclude that the network provides well-defined lithium sites which are separated by barriers larger as compared to k_BT. The lithium ions basically jump between adjacent sites. The term *jump* implies that the time scale it takes to cross the saddle is much shorter than the time scale the ions fluctuate within the individual sites. This conclusion is in qualitative agreement with previous simulations [15, 24, 40, 41, 42] and also agrees with the appearance of the trajectories in Fig.1.
The first minimum of $G_s(r,t)$ around $r_{min} \approx 1.5$ Å can be used to distinguish local vibrational dynamics ($|\Delta r(t)| < 1.5$ Å) and long-range dynamics ($|\Delta r(t)| > 1.5$ Å). Of course, there may be individual ions which display local fluctuations with a length scale larger than 1.5 Å. On average, however, this value of 1.5 Å turns out as a significant length scale in the above-mentioned sense. This scenario of jumps between well-defined potential wells implies that the ions explore the individual sites for rather long times before they leave the site on a time scale approximately given by the decay time of $S(q_{max},t)$. In order to analyse the intra-site dynamics somewhat closer we have determined the mean square displacement $\langle r^2(t) \rangle_{local}$ of those particles which at time t have moved less than 1.5 Å. This curve is shown at all four temperatures of our study in Fig.10. For times larger than 0.2 ps $\langle r^2(t) \rangle_{local}$ starts to become constant. This means that already on this short time scale the lithium ions have largely explored the local potential well. The increase of $\langle r^2(t) \rangle_{local}$ for $T = 1240$ K at long times is related to the fact that the network starts to relax since we are above its glass transition temperature. Note that the temperature dependence of this local exploration time is very weak. A careful inspection shows that for the two lower temperatures there is further gradual increase until $t \approx 10$ ps ($T = 750$ K) and $t \approx 100$ ps ($T = 640$ K), respectively. This observation indicates the presence of a substructure of the different wells. At low temperatures the exploration of the initial well might require the crossing of some lower saddles. This would explain the slower approach to the final plateau value as compared to the dynamics in a smooth local potential.

For long times all curves approach a constant plateau value $\langle r^2(t \to \infty)\rangle_{local}$. An exception is $T = 1240$ K where we take the value around $t = 10$ ps. In Fig.11 this plateau value is plotted against temperature. To a good approximation $\langle r^2(t \to \infty)\rangle_{local}$ is proportional to temperature. This is expected for the dynamics in a harmonic potential. Thus the local dynamics can be characterized by an effective harmonic potential. These local fluctuations are related to the Debye-Waller factor [43].

Now we are in a position to discuss $w(t)$. The lengthscale $r_{min} = 1.5$ Å as derived from the van Hove self correlation function allows us to separate local and long-range motion and was the basis to study $\langle r^2_{local}(t)\rangle$. In analogy to $w(t)$ we define

$$w_{local}(t) \equiv (d/dt)\langle r^2_{local}(t)\rangle. \tag{13}$$

It is shown in Fig.12 at different temperatures. The temperature dependence of w_{local} is rather weak. For $t > 20$ fs it roughly scales like t^{-2}.

In Fig.13 $w(t)$ is shown for several temperatures. Three different time regimes can be distinguished. (i) For $t < 20fs$ there is the ballistic regime, i.e. $w(t) \propto t$. (ii) For $20fs < t < 1ps$ there is a strong decay of $w(t)$. (iii) For $t > 1ps$ $w(t)$ decays much slower until it becomes constant for large times. Whereas for $T = 1240$ K and $T = 980$K this final decay is very weak it becomes significantly larger for lower temperatures. For $T = 640$ the decay spans even more than a decade.

It is instructive to compare this with the typical experimental $\sigma(\nu)$ data for alkali silicates, as already discussed in the Introduction. The frequency regimes there have a one-to-one correspondence to the characteristic time regimes of $w(t)$. (i) The vibrational modes for $\nu > 10^{13}$ Hz correspond to the ballistic regime in the time domain. Since $1/(\pi^2\nu) \approx 10fs$ this agrees very well with the corresponding time regime of $w(t)$ (ii) As mentioned before the $\sigma(\nu) \propto \nu^2$ behavior for 10^{13} Hz$> \nu > 10^{11}$ Hz can be attributed to stochastic dynamics in a harmonic potential [8]. For the time dependence of $w(t)$ of an overdamped vibration one expects $w(t) \propto \exp(-kt)$ with some decay constant k [44]. For a complicated system like an amorphous ion conductor a distribution of decay constants should be present, resulting in a somewhat modified decay characteristics, but still yielding $\sigma(\nu) \propto \nu^2$ for $\nu < 1/k_{max}$ as obtained via Fourier transformation. Here k_{max} denotes the upper cutoff of the distribution of decay constants. In any event, one expects a very strong decay in agreement with the behavior in $w(t)$ for times $20fs < t < 1ps$. (iii) The more gradual decrease of $\sigma(\nu)$ for $\nu < 10^{11}$ is also recovered in our simulated $w(t)$ curves for the two lower temperatures. For $T \geq 950$ K $w(t)$ is roughly constant for $t > 1ps$. For the sodium silicate system the dispersion of $\sigma(\nu)$ as roughly expressed by $\sigma(\nu \approx 10^{11}Hz)/\sigma_{dc}$ is about 10^7 at room temperature. It becomes smaller with increasing temperature and vanishes at around $T \approx 900$ K.

The postulation of a crossover from vibrational-type to long-range dynamics around $\nu = 10^{11}$ Hz, as derived from conductivity spectra, is consistent with physical intuition. There is, however, no strict derivation. Here simulations may give additional information because the micro-

scopic nature of dynamics is known in detail. In particular, we have identified the contribution $w_{local}(t)$ which arises from local vibrational dynamics, see Fig.12. As expected its value is close to $w(t)$ for short times. The long-range contribution to $w(t)$ can be estimated as $w(t) - w_{local}(t)$. This is included in Fig.13 for the two lowest temperatures. For these temperatures one can clearly see that the dispersion for $t > 1ps$ is mainly due to long-range motion. For $T = 640$ K the dispersion, i.e. $w(t = 1ps)/w(t \to \infty)$, is around 20.

4 Discussion and Summary

The analysis as presented above allows us to improve our understanding of the frequency dependence of the conductivity. Here it is helpful that the time-dependence of $w(t)$ (derivative of the mean square displacement) is strongly related to the frequency dependence of $\sigma(\nu)$. As outlined above several findings like the activation energy or the Haven ratio are in good agreement with the corresponding results of experiments. In particular it turns out that only for temperatures below 900 K the system displays dispersive dynamics due to long-range dynamics. Thus only simulations in the nanosecond regime can cope with the effect of back- and forthjumps as observed in the experiment. At first view this result disagrees with the fact that even at $T = 1240$ K the mean square displacement (see Fig.4) is not diffusive but shows a subdiffusive regime. Our analysis of $w(t)$, however, has revealed that the subdiffusive regime for this high temperature is related to local vibrational dynamics. Therefore it only contributes to the high-frequency regime of $\sigma(\nu)$, reflecting vibrational properties.
Long-range dynamics prevails for $t > 1$ ps or, correspondingly, $\nu < 10^{11}$ Hz. This observation seems to contradict the conclusion in Ref.[45] that the nearly constant loss and thus the dynamics for frequencies much lower than 10^{11} Hz is due to anharmonic vibrational dynamics rather than jump dynamics. A priori, however, it is not clear whether long-range dynamics automatically implies jump-like motion and further work is necessary to clarify this point.
As shown in Fig.13 the subtraction of $w_{local}(t)$ from $w(t)$ yields a plateau-like region for short times. This is in agreement with recent work on amorphous 0.5 Ag_2S - 0.5 GeS_2 [8]. Of course, for experimental data it is not possible to determine the vibrational contribution individually. For some materials, however, it can be estimated reliably [8]. The interpretation of $w(t) - w_{local}(t)$ as the contribution of jumps between discrete sites is definitely justified for long times. In general it is justified as long as the vibrational and the jump dynamics are uncorrelated to each other. Intuitively one would expect that this is the case for time scales which are significantly longer than the time it takes for the ion to transfer between two adjacent sites. Two important questions remain. What is this crossing time? What is the physical interpretation of $w(t) - w_{local}(t)$ for shorter times than the crossing time? Work along this line is in progress.
Another important aspect is related to the time-temperature superposition principle. The scaling, observed in Fig.6, is consistent with the Summerfield scaling as can be easily checked

with the help of Eq.1. As is evident from Eq.1 measurement of $\sigma(\nu)$ is not sufficient to obtain an absolute value of the mean square displacement. From measurements of $\epsilon'(\infty)$, however, it becomes possible to get information about the absolute value $c(T)$ of $\langle r^2(t)\rangle$ for short times (or high frequencies, respectively) where only the local fluctuations contribute [3, 4, 49]. In agreement with our results (see Fig.11) one finds to a good approximation $c(T) \propto T$ [49]. A more detailed comparison of the experimental scaling results and our findings for the mean square displacement is not possible so far since our scaling regime is still very limited and simulations at still lower temperatures had to be taken into account.

Finally, we would briefly comment on the different activation energies of the conductivity and the incoherent scattering function. In glass-forming systems at low temperatures a similar effect is seen when comparing the rotational correlation function (which basically behaves like the translational incoherent scattering function) and the diffusion constant. As explained in Ref.[46] such an effect may be related to a broadening of the waiting time distribution for decreasing temperature. The diffusion constant is mainly dominated by the fast ions. In contrast, decay of the incoherent scattering function (with time scale τ) requires that also the slow ions move. Thus an increase of heterogeneity would increase the product of the diffusion constant and the relaxation time τ. On a qualitative level this is seen in our simulations. Although the heterogeneities indeed increase with decreasing temperature [47] we do not know whether this is the only explanation for the different activations energies. In any event, this question is accessible experimentally since via multidimensional NMR observables can be measured which are believed to behave like the incoherent scattering function [48].

The increase of heterogeneity as indirectly seen by the different activation energies implies that in a very strict sense the dynamics at lower temperatures is not a simple time-scaled version of the dynamics at higher temperatures. Thus we have to conclude that the mean square displacement and the incoherent scattering function, which both can be interpreted as reduced representations of the dynamics, are not sensitive to these deviations from time-temperature superposition. Actually, a similar observation has been already reported for a glass-forming hard sphere system for which the non-gaussian parameter strongly depends on density although the mean square displacement displays time-density superposition [50].

Several important questions remain to be answered. How do the observed features correlate with the local network structure (see Refs.[18, 19] for interesting features observed recently)? To which degree do the observed features change with concentration? What can one learn about the nature of correlated back- and forthjumps? For the latter question it turns out to be very helpful to study appropriate three-time correlation functions [47].

Of course, the results of several experiments as well as previous simulations already contain part of the answers. However, since computer simulations are always dealing with temperatures much higher than experiments one has to be very careful to extract information from simulations which is relevant for experiments. Therefore the advent of faster computers and thus the ability to simulate at sufficiently low temperatures will render computer simulations of ion conductors

a fruitful field for the future.

5 Acknowledgement

In this work we have greatly benefited from helpful discussions with C. Cramer, K. Funke, J. Horbach, and B. Roling. We acknowledge the support by the DFG (SFB 458). Furthermore we would like to acknowledge K. Refson for supplying the MOLDY software package.

References

[1] K. Funke, R.D. Banhatti, S. Brückner, C. Cramer, C. Krieger, A. Mandanici, C. Martiny and I. Ross (this volume).

[2] J. C. Dyre and T. B. Schroder, Rev. Mod. Phys., 2000, **72**(39), 873.

[3] B. Roling, C. Martiny and K. Funke, J. Non-Cryst. Solids, 1999, **249** (2-3), 201.

[4] B. Roling, C. Martiny and S. Brückner, Phys. Rev. B, 2001, **63**, 214203.

[5] D. Knödler, P. Pendzig and W. Dieterich, Solid State Ionics, 1996, **86-88**, 29.

[6] P. Maass, M. Meyer, A. Bunde and W. Dieterich, Phys. Rev. Lett., 1991, **77**, 1528.

[7] T. Wong, C.A. Angell eds., Glass structure by spectroscopy, 1976, Marcel Dekker, New York.

[8] C. Cramer, S. Brückner, Y. Gao, K. Funke, R. Belin, G. Taillades and A. Pradel (J. Non-Cryst. Solids, in press).

[9] S. Summerfield, Phil. Mag. B, 1985, **52**, 9.

[10] Y. Haven and B. Verkerk, Phys. Chem. Glasses, 1965, **6**, 38.

[11] J.O. Isard, J. Non-Cryst. Solids, 1999, **246**, 16.

[12] R. Kubo, J. Phys. Soc. Japan, 1957, **12**, 570.

[13] J. Habasaki, I. Okada and Y. Hiwatari, Phys. Rev. E, 1995, **52**(3), 2681.

[14] J. Habasaki, I. Okada and Y. Hiwatari, Molecular Simulation, 1993, **10**(1), 19.

[15] B. Park and A. N. Cormack, J. Non-Cryst. Solids, 1999, **255**, 112.

[16] J. Horbach and W. Kob, Phil. Mag. B, 1999, **79**, 1981

[17] J. Horbach, K. Binder and W. Kob, J. Chem. Geol., 2001, **87**, 174

[18] P. Jund, W. Kob and R. Jullien, Phys. Rev. B., 2001, **64**, 134303.

[19] J. Horbach, W. Kob and K. Binder, Phys. Rev. Lett. 2002, **88**, 125502.

[20] J. Oviedo and J. F. Sanz, Phys. Rev. B, 1998, **58** (14), 9047.

[21] X. Yuan and A. N. Cormack, J. Non-Cryst. Solids, 2001, **283**, 69.

[22] M.A. Manalang, D.B. Bergstrom, D.E. Kramer and J. Kieffer, J. Non-Cryst. Solids, 1994, **169**, 72.

[23] J. Kieffer, J. Non-Cryst. Solids, 1994, **172-174**, 1285.

[24] W. Smith, G.N. Greaves and M.J. Gillan, J. Chem. Phys., 1995, **103**, 1995.

[25] W. Smith, T. R. Forester, G. N. Greaves, S. Hayter and M. J. Gillan, J. Mater. Chem., 1997, **7**, 331.

[26] R.D. Banhatti and A. Heuer, Phys. Chem. Chem. Phys., 2001, **3** 5104.

[27] J. Habasaki, Molecul. Phys., 1990, **70**(3), 513.

[28] J. Habasaki and I. Okada, Molecular Simulation, 1992, **9**(5), 319.

[29] J. Habasaki, I. Okada and Y. Hiwatari, J. Non-Cryst. Solids , 1992, **183**, 12.

[30] H. Doweidar, J. Non-Cryst. Solids, 1996, **194**, 155.

[31] K. Refson, Computer Physics Communications, 2000, **126** (3), 310.

[32] B. Gee and H. Eckert, Solid State Nucl. Magn. Reson., 1995, **5**, 113.

[33] G.N. Greaves, Y. Vaills, S. Sen and R. Winter, J. of Optoelec. and Adv. Mat., 2000, **2**, 299.

[34] A. Bunde, M. D. Ingram and P. Maass J. Non-Cryst. Solids, 1994, **172-174**, 1222.

[35] W. Götze and L. Sjögren, Rep. Prog. Phys., 1992, **55**, 241.

[36] W. Kob and H.C. Andersen, Phys. Rev. E, 1995, **51**, 4626.

[37] B. Doliwa and A. Heuer, Phys. Rev. E, 2000, **61**, 6898.

[38] J. Habasaki, I. Okada, and Y. Hiwatari, Phys. Rev. B, 1997, **55**, 10.

[39] J. P. Hansen and I. R. McDonald, 1986, *Theory of Simple Liquids*, Academic Press, London.

[40] A. N. Cormack and Y. Cao, Molec. Eng. 1996, **6**, 183.

[41] J. Habasaki, J. Non-Cryst. Solids, 1995, **12**, 183.

[42] S. Balasubramanian and K. J. Rao, J. Phys. Chem., 1994, **98**, 10871.

[43] C.A. Angell, Solid State Ionics, 1998, **105**, 15.

[44] M. Doi, S.F Edwards, 1986, *The Theory of Polymer Dynamics*, Oxford University Press, Oxford.

[45] C. Leon, A. Rivera, A. Varez, J. Sanz, J. Sanatamaria and K.L. Ngai, Phys. Rev. Lett., 2001, **86**, 1279.

[46] G. Diezemann, H. Sillescu, G. Hinze and R. Böhmer, Phys. Rev. E, 1998, **57**, 4398.

[47] A. Heuer, M. Kunow, M. Vogel and R.D. Banhatti (in preparation).

[48] M. Vogel, C. Brinkmann, H. Eckert and A. Heuer (this volume).

[49] A. Happe, PhD-thesis, Münster (1997).

[50] B. Doliwa and A. Heuer, J. Phys.: Condens. Matter, 1999, **11**, A277.

Fig. 1 Trajectories of three different lithium ions at $T = 750$ K as projected on a plane. The box length is 9 Å.

Fig. 2 The partial structure factor $g(r)$ for the lithium ions at different temperatures.

Fig. 3 The integrated partial structure factor $h(r)$ for the lithium ions at different temperatures.

Fig. 4 The mean square displacement $\langle r^2(t)\rangle$ for lithium at different temperatures.

Fig. 5 The temperature dependence of the diffusion constant of Li_2O SiO_2. The data marked as circles have been taken from Ref.[26].

Fig. 6 The same as in Fig.4. The individual times have been scaled in order to show the time-temperature superposition.

Fig. 7 The time dependence of the incoherent scattering function $S(q,t)$ for $q = q_{max} = 2\pi/d_0$ at different temperatures. The broken lines correspond to a fit with the KWW function $A\exp(-(t/\tau)^\beta)$ with $\beta = 0.45$.

Fig. 8 The time dependence of dynamic cooperativity as expressed by $N_{coop}(t)$ for different temperatures.

Fig. 9 The self part of the van Hove correlation function $G_s(r,t)$ for different times t at $T = 750$ K.

Fig. 10 The local mean square displacement $\langle r^2(t)\rangle_{local}$ which averages over all displacements less than $r_{min} = 1.5$ Å.

Fig. 11 The temperature dependence of $\langle r^2(t\to\infty)\rangle_{local}$.

Fig. 12 $w_{local}(t)$ at different temperatures.

Fig. 13 $w(t)$ at different temperatures. For the two lowest temperatures also $w(t) - w_{local}(t)$ is displayed.

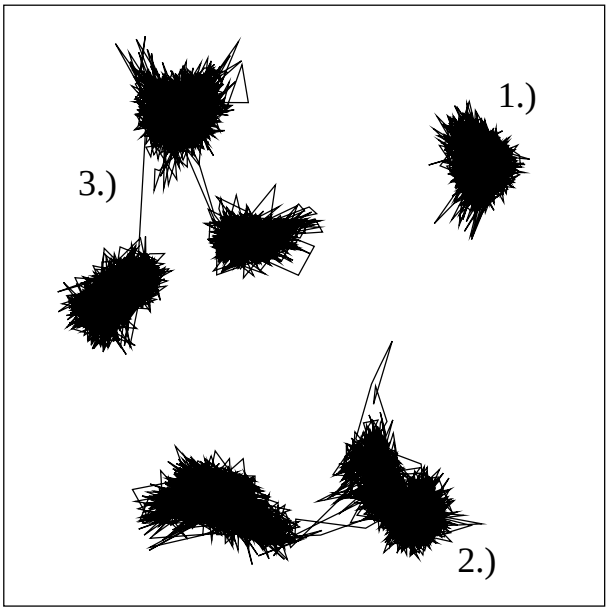


Fig. 1

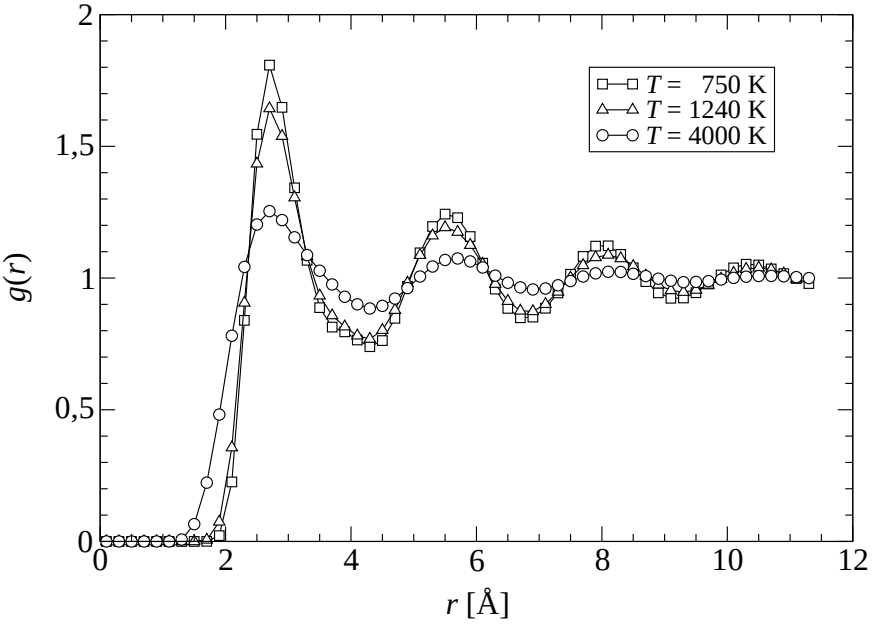


Fig. 2

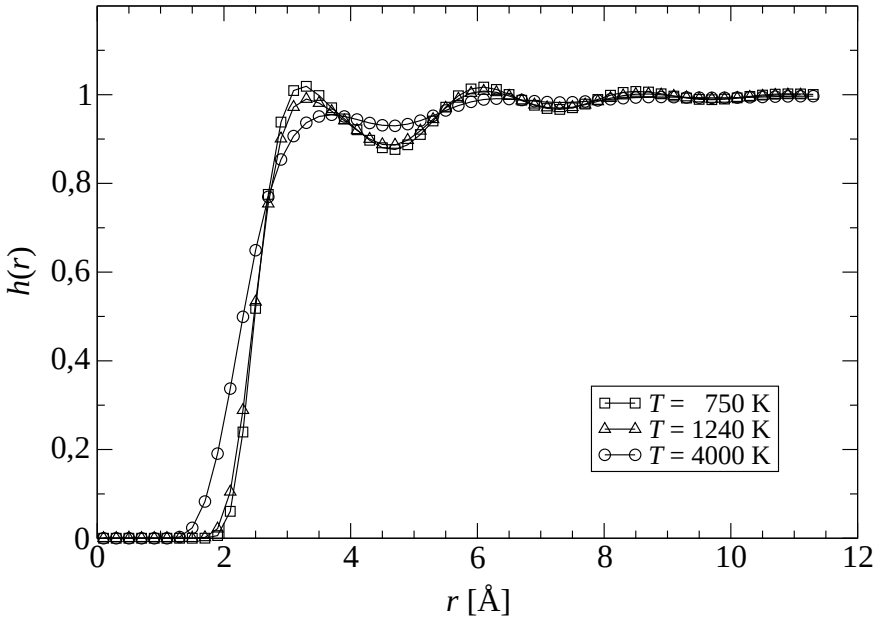

h(r)
r [Å]
T = 750 K
T = 1240 K
T = 4000 K

Fig. 3

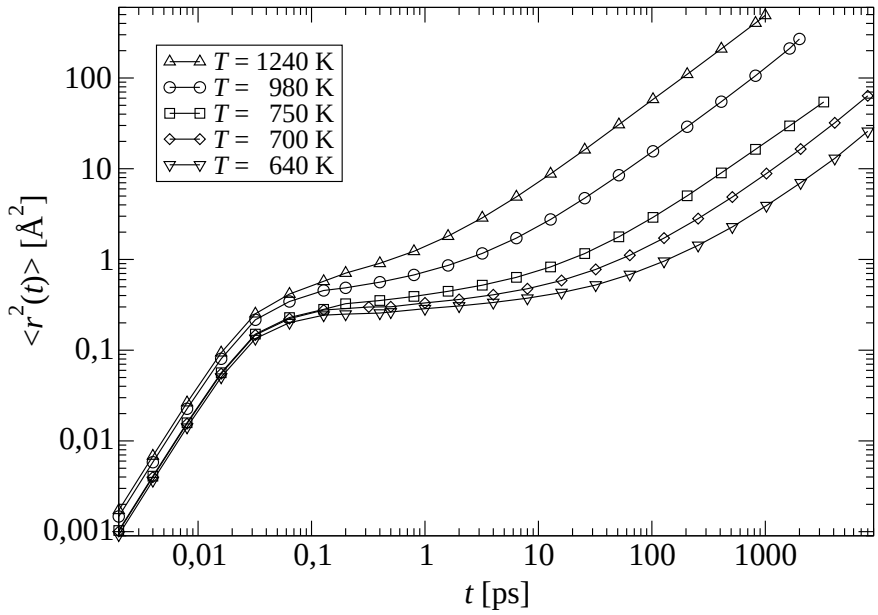

<r²(t)> [Å²]
t [ps]
T = 1240 K
T = 980 K
T = 750 K
T = 700 K
T = 640 K

Fig. 4

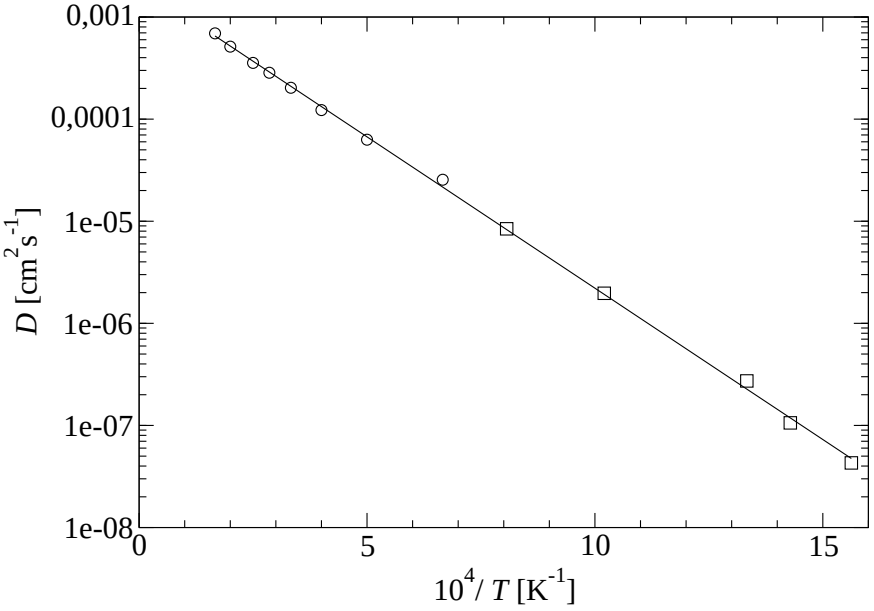

0,001
0,0001
1e-05
1e-06
1e-07
1e-08
D [cm2 s-1]
0
5
10
15
10^4/ T [K^-1]

Fig. 5

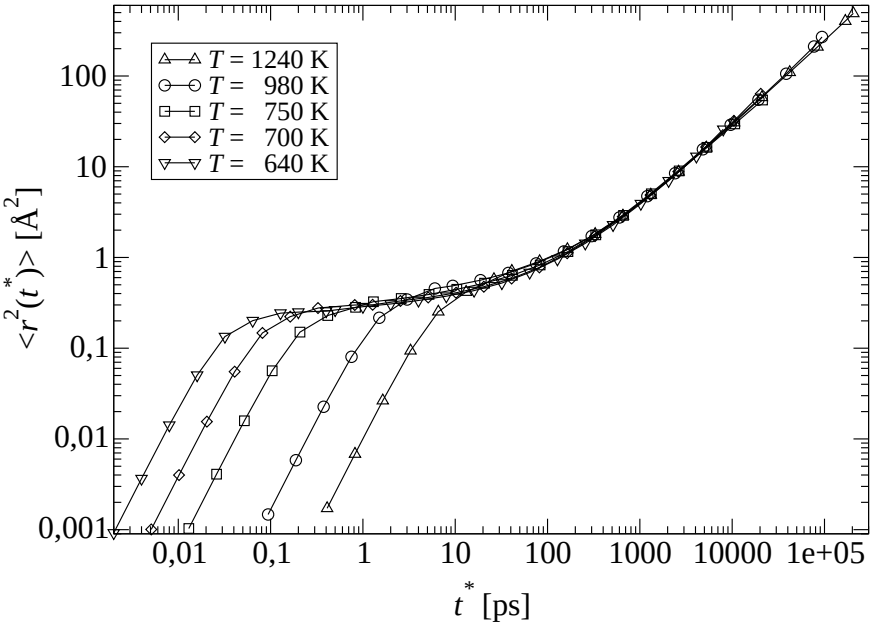

T = 1240 K
T = 980 K
T = 750 K
T = 700 K
T = 640 K
100
10
1
0,1
0,01
0,001
<r2*(t*)> [Å2]
0,01
0,1
1
10
100
1000
10000
1e+05
t* [ps]

Fig. 6

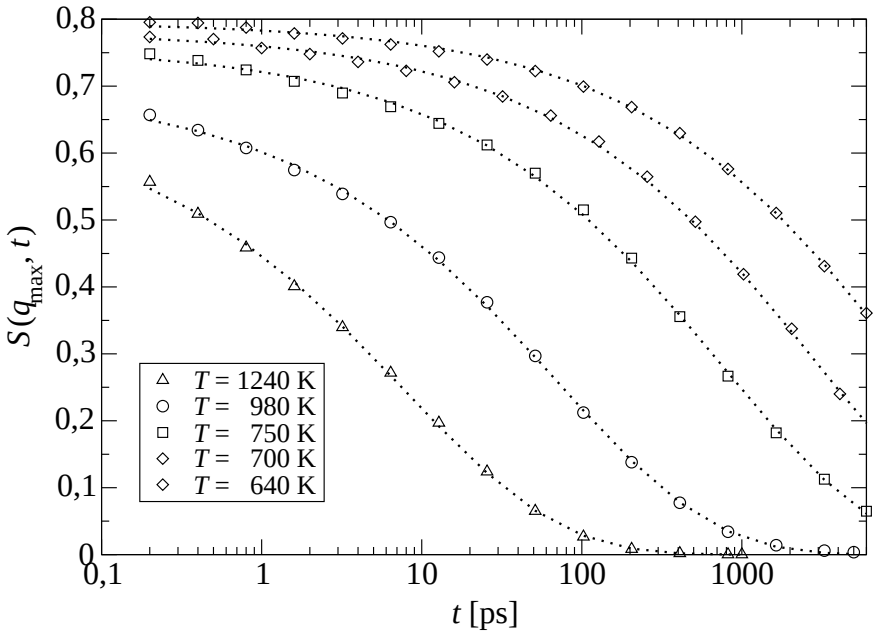

0,8
0,7
0,6
0,5
0,4
0,3
0,2
0,1
0
0,1
1
10
100
1000
$S(q_{max}, t)$
t [ps]
T = 1240 K
T = 980 K
T = 750 K
T = 700 K
T = 640 K

Fig. 7

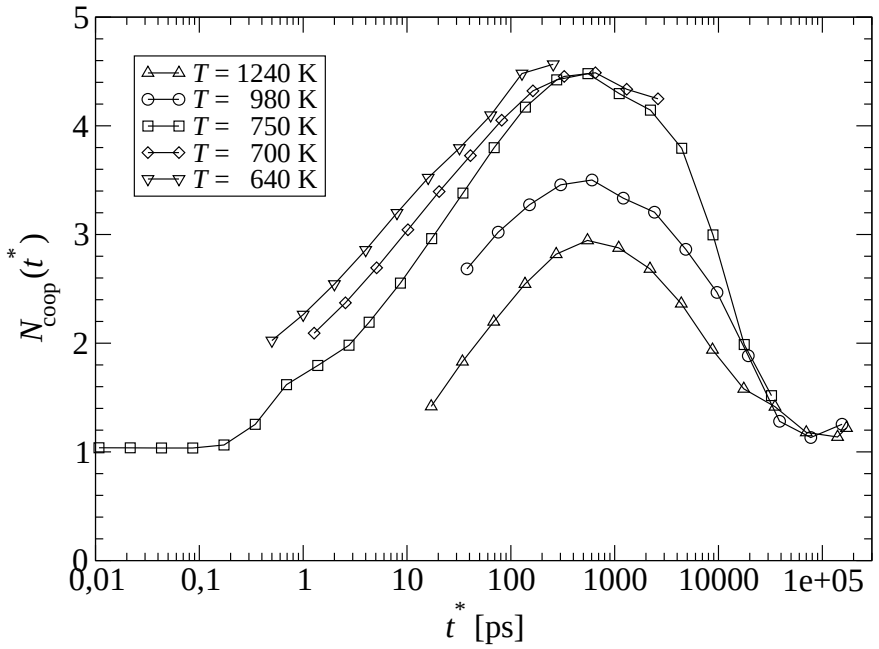

5
4
3
2
1
0
0,01
0,1
1
10
100
1000
10000
1e+05
$N^*_{coop}(t^*)$
t^* [ps]
T = 1240 K
T = 980 K
T = 750 K
T = 700 K
T = 640 K

Fig. 8

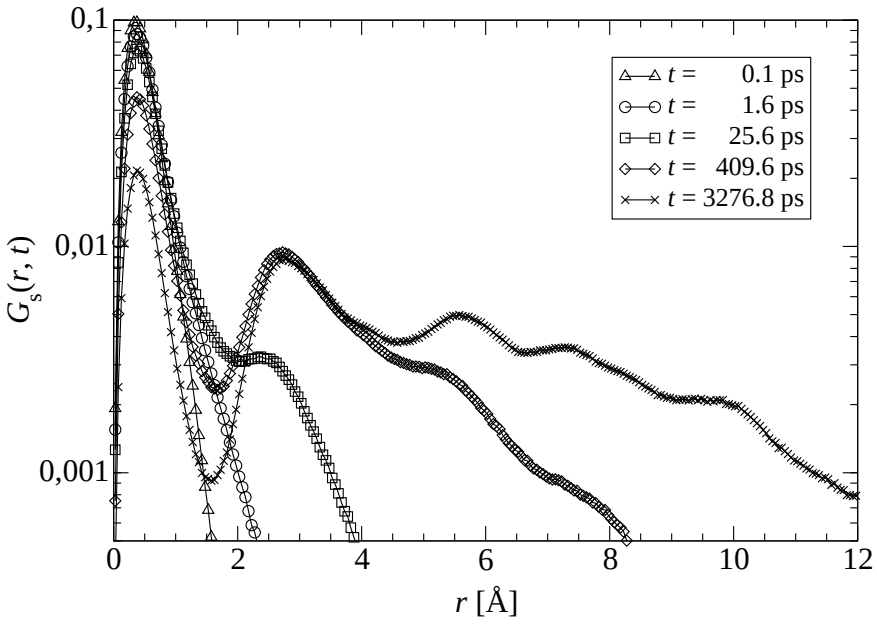

0,1
0,01
0,001
$G_s(r,t)$
0
2
4
6
8
10
12
r [Å]
t = 0.1 ps
t = 1.6 ps
t = 25.6 ps
t = 409.6 ps
t = 3276.8 ps

Fig. 9

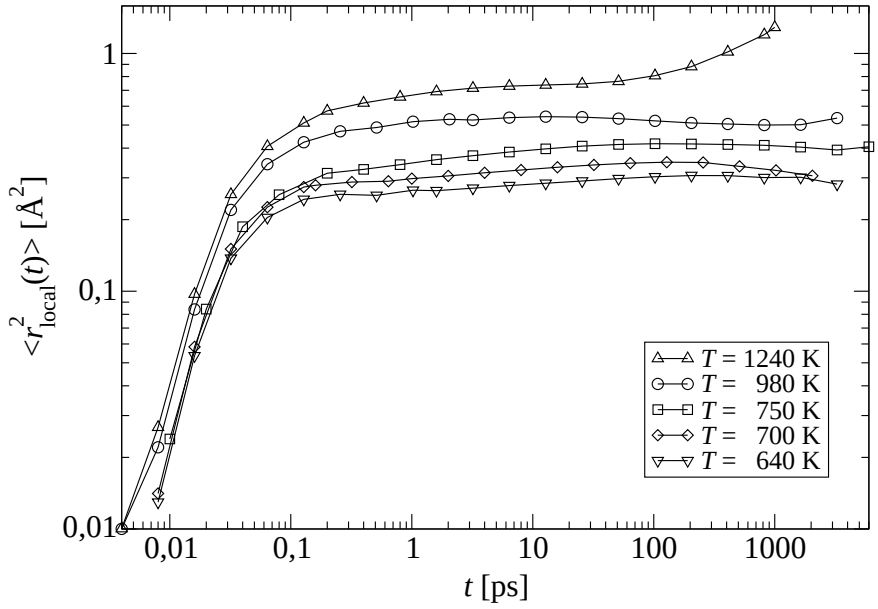

1
0,1
0,01
$<r^2_{local}(t)>$ [Å^2]
0,01
0,1
1
10
100
1000
t [ps]
T = 1240 K
T = 980 K
T = 750 K
T = 700 K
T = 640 K

Fig. 10

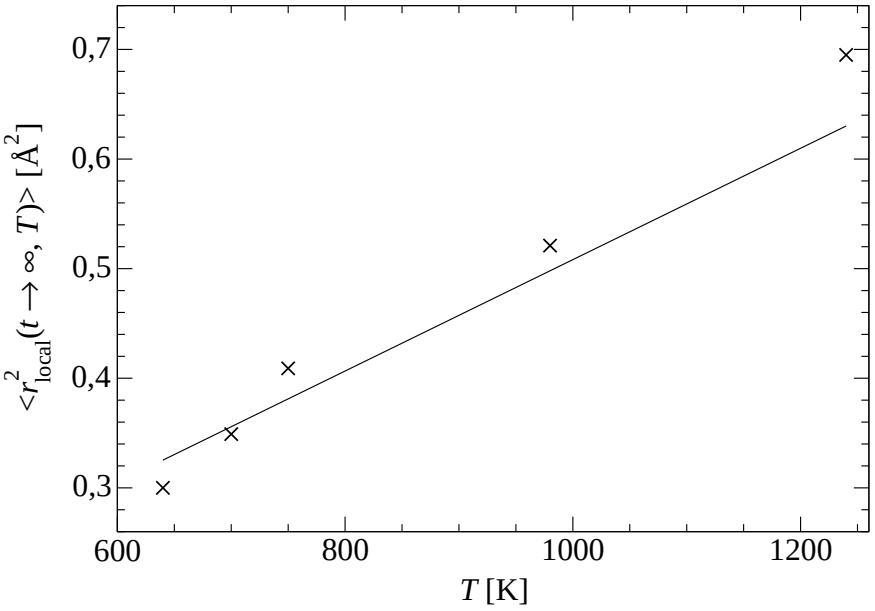

0,7
0,6
0,5
0,4
0,3
600
800
1000
1200
T [K]
$<r^2_{local}(t \to \infty, T)>$ [Å^2]

Fig. 11

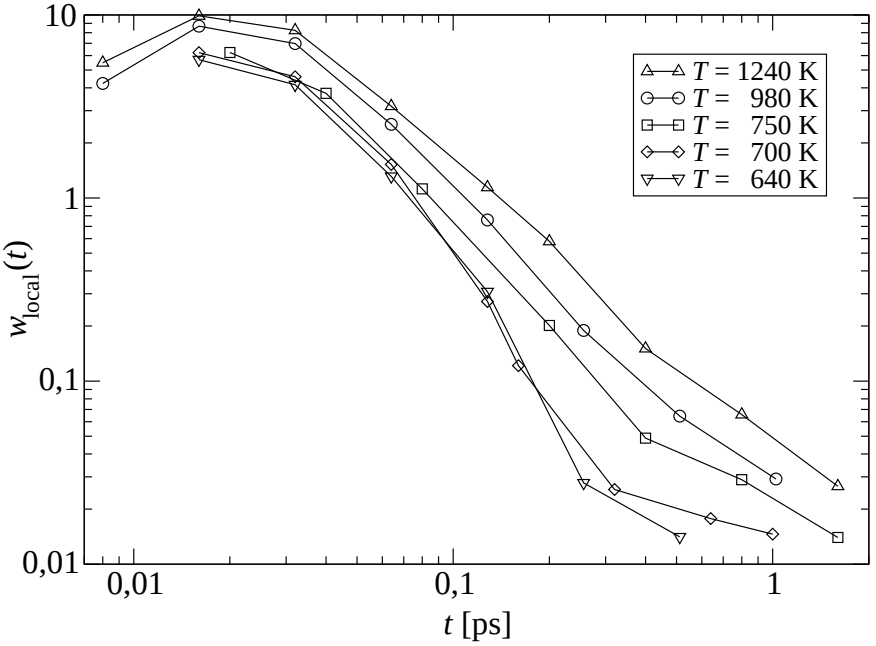

10
1
0,1
0,01
0,01
0,1
1
t [ps]
$w_{local}(t)$
T = 1240 K
T = 980 K
T = 750 K
T = 700 K
T = 640 K

Fig. 12

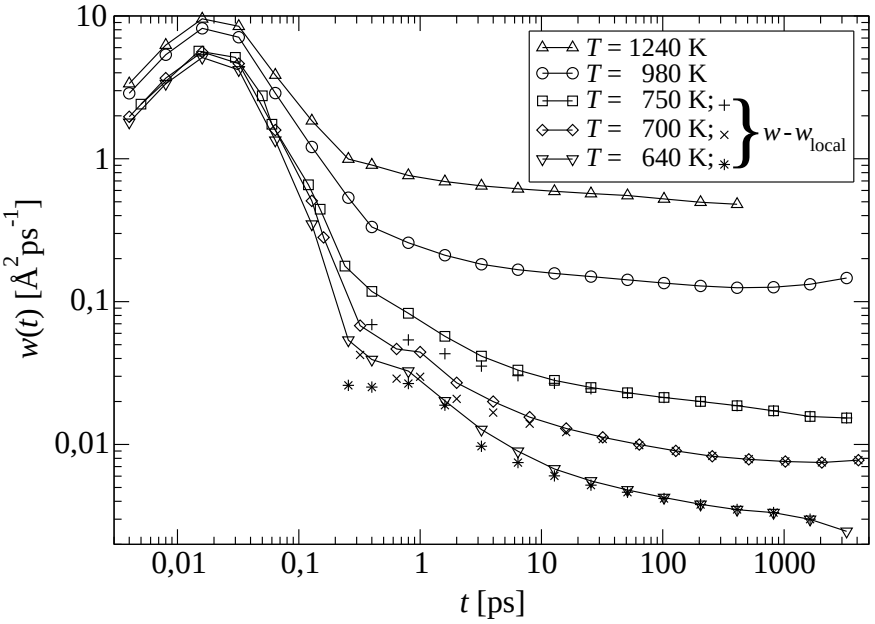

10
1
0,1
0,01
0,01
0,1
1
10
100
1000
w(t) [Å^2 ps^-1]
t [ps]
T = 1240 K
T = 980 K
T = 750 K; +
T = 700 K; ×
T = 640 K; *
w - w_local

Fig. 13